complexities

MDPI

Article

The Noise-Perturbed Onset of Chaos as a Model for Dissolution of Congested Vehicle Traffic

Santa Elena Tellez-Flores [1,2] and Alberto Robledo [2,*]

[1] Universidad Nacional Rosario Castellanos, Avenida 506 0riente, Mexico City 07979, Mexico; santatellez26@rcastellanos.cdmx.gob.mx
[2] Instituto de Física, Universidad Nacional Autónoma de México, Ciudad Universitaria, Mexico City 04510, Mexico
* Correspondence: robledo@fisica.unam.mx

Abstract

We present a nonlinear dynamical model for vehicular traffic jams and their dissolution based on the noise-perturbed onset of chaos. The model makes use of the bifurcation gap generated by addition of noise to quadratic iterated maps. The gap results from the elimination by noise of periodic and chaotic attractors with large periods and large numbers of chaotic bands, respectively. The bifurcation gap is recapitulated at the transition to chaos (vanishing Lyapunov exponent) as a crossover from noiseless to irregular, chaotic-like regimes at an iteration time t_{cross} with value dependent on the noise amplitude. This behavior is employed in a model (with variants) that we design for multilane road congested traffic. We highlight four main model properties that are also present in the dynamics of glass formation: (i) plateau interrupted relaxation; (ii) Adam–Gibbs empirical law; (iii) aging; and (iv) diffusion arrest. The model bridges previous studies that have indicated analogies between glassy dynamics and vehicular traffic as well as nonlinear dynamics and same-name traffic. We also discuss the connection of the model with urban multilane road networks.

Keywords: vehicular traffic; nonlinear dynamics; logistic map; additive noise; bifurcation gap; onset of chaos; glassy dynamics

1. Introduction

Traffic congestion in densely populated urban areas is inextricably connected to economic, social and environmental consequences. There exist many well-known mitigation strategies, which include automated, infrastructural, social, and eco-friendly characteristics [1,2]. The complexity of this subject becomes evident when the reasons for the shortages and inefficiencies of existing remedies are considered.

The research literature of modeling real-world vehicle traffic is very diverse and to describe either its development over time, or its current state, requires detailed knowledge and time. It is not our purpose here to do so, particularly because our objective, described below, is only to offer the elements of a unique approach, very different from mainstream models and methods, that is suited to uncovering the underlying physics shared by complex systems of very different natures when they suffer a severe impediment to access their otherwise normal set of configurations [3], with glasses and congested traffic among them.

However, we mention recent reviews of vehicle traffic models and methods that help us and the interested reader to obtain an overview. These models and methods appear

Check for updates

Academic Editors: José F. F. Mendes and Liang Gao

Received: 29 June 2026
Revised: 13 August 2026
Accepted: 21 August 2026
Published: 26 August 2026

Copyright: © 2026 by the authors. Licensee MDPI, Basel, Switzerland. This article is an open access article distributed under the terms and conditions of the Creative Commons Attribution (CC BY) license.

in two categories according to the scale that they look at traffic from: microscopic [4,5], tracking the behavior of individual vehicles, and macroscopic [6,7], treating traffic as a continuous fluid. Our model presents three variants, two microscopic and one macroscopic, where the former provides dynamical properties within a multilane road and the latter is different from hydrodynamics but based on diffusion.

Here, we ignore the interdisciplinary consequences of congested traffic mentioned, as well as specific comparisons with existing models, and focus ourselves only on the most basic exercise within the framework of current efforts within theoretical research in complex systems [3]. Our aim is limited to the development of a tractable mathematical model capable of capturing some general behaviors of congested vehicular traffic. Our main objective here is to substantiate that the general behaviors obtained are formally analogous to well-known properties of glass formation in molecular systems; see Figure 1. The benefits lie only in the full understanding of a simple model, while the shortcomings are related to its present disconnection from applied research.

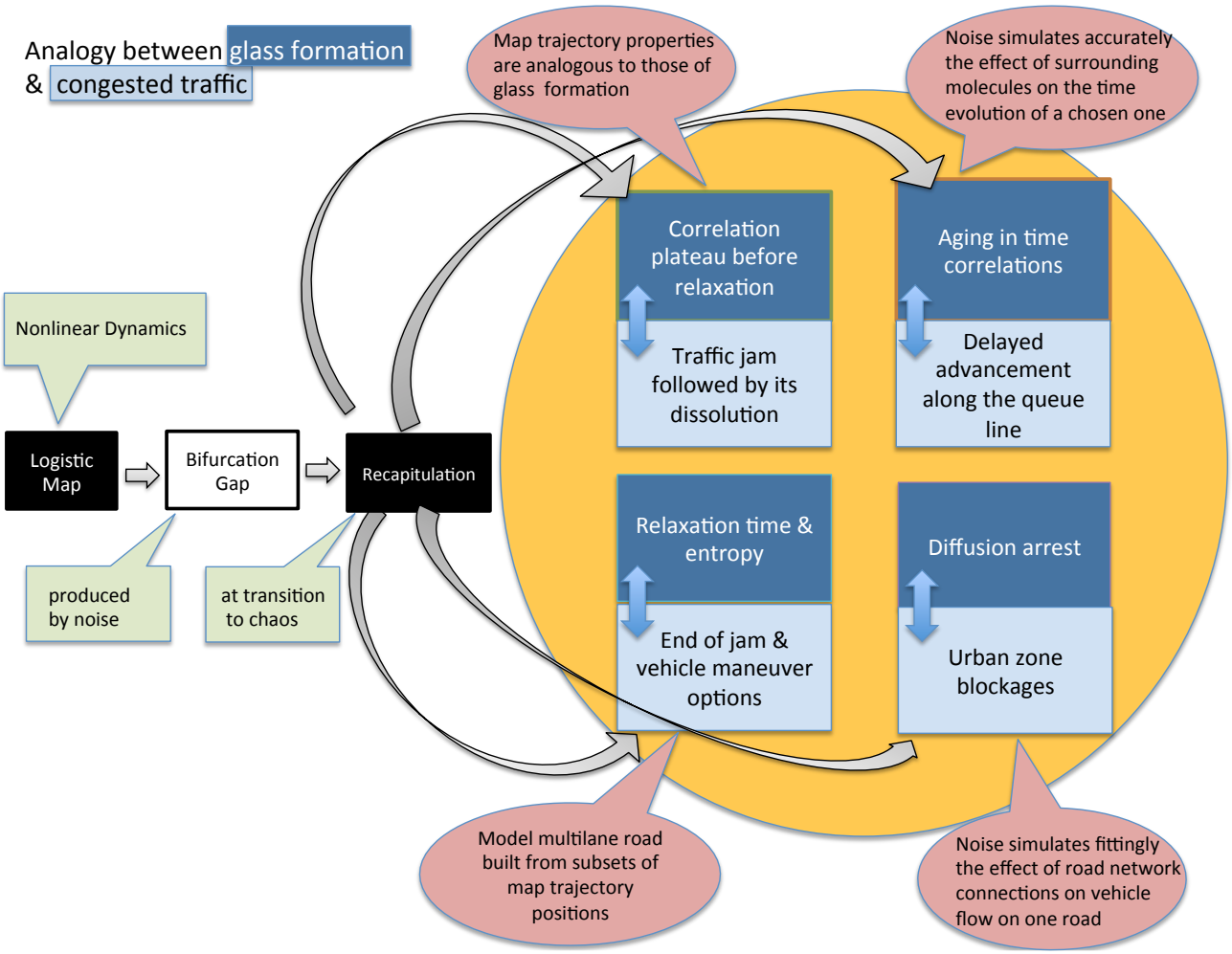


Figure 1. Overall structure diagram of our study based on nonlinear dynamics that demonstrates a robust analogy between glass formation and congested traffic. See text for details.

Our model is based on the nonlinear dynamics of dissipative iterated maps [8–10]. We choose the classic, one-dimensional, logistic map [8–11] perturbed with additive noise [8–10,12]. This hybrid deterministic–stochastic model system was studied more than four decades ago. We recall here the main property found at that time: the bifurcation gap [8–10,12]. The addition of noise suppresses periodic attractors of periods larger than $2^{N(\sigma)}$ as well as chaotic-band attractors with a number of bands larger than $2^{N(\sigma)}$, where

$N(\sigma)$ is a decreasing function of the noise amplitude σ. We recall too [8–10] that the original noiseless bifurcation diagram (or its collection of attractors ordered with increasing values of its control parameter denoted μ) of the logistic map exhibits a period-doubling cascade of regular attractors of periods 2^n as well as a band-splitting cascade of chaotic attractors of 2^n bands. The common accumulation point $n \to \infty$ of both cascades coincides at the so-called transition to (or out of) chaos [8–10]. We also remember that the Lyapunov exponent λ is negative for periodic attractors, positive for chaotic ones and vanishes at the transition to chaos [8–10]. The addition of noise shortens the two cascades that now appear joined at the finite maximum $2^{N(\sigma)}$ period or chaotic-band number at which the Lyapunov exponent $\lambda(N(\sigma)) = 0$ again vanishes as it changes sign. This is the bifurcation gap, and an interesting feature of it is that the transition to chaos (that separates converging to diverging trajectories) persists for the noise-perturbed map [8–10,12]; see Figure 2.

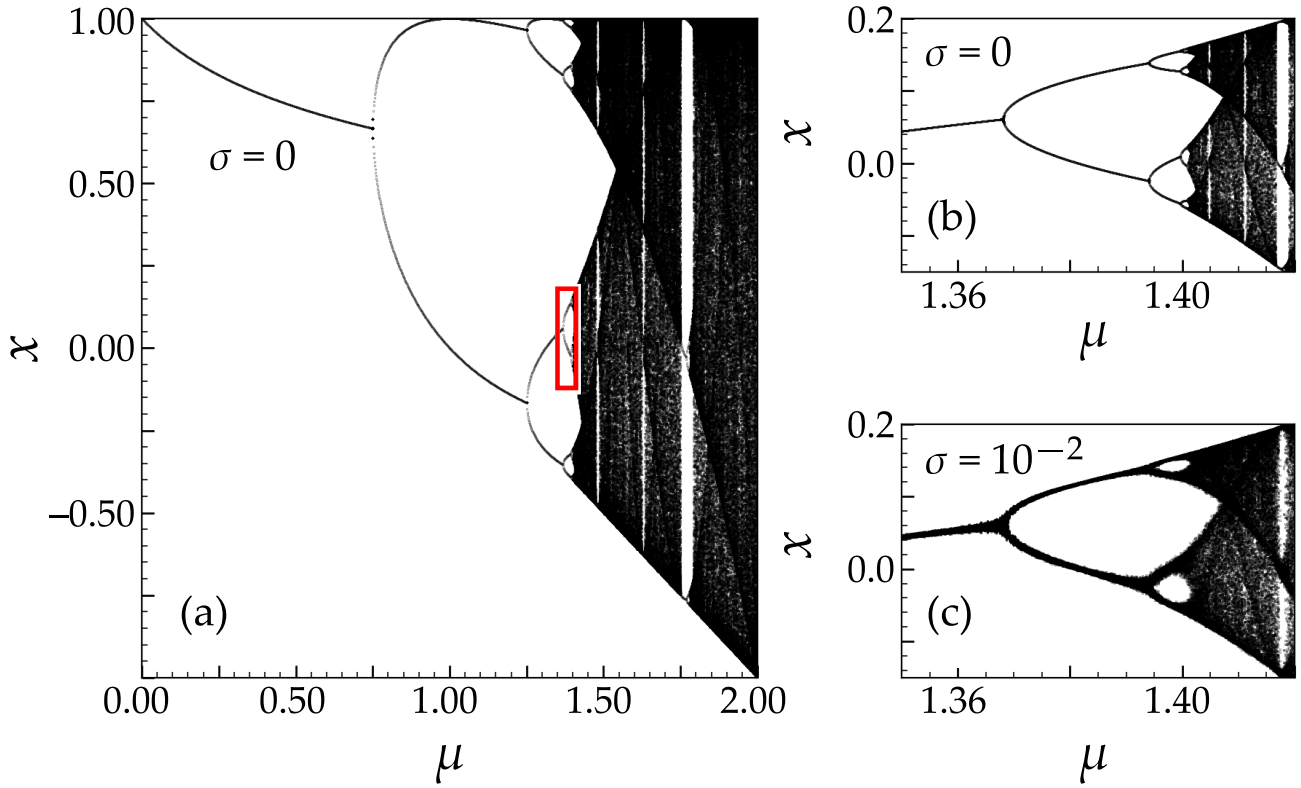


Figure 2. (**a**) The bifurcation diagram of the logistic map as generated by Equation (1) with noise amplitude $\sigma = 0$, where μ is the control parameter. (**b**) Magnification of the box in (**a**), and, in contrast, the modification produced by noise of the same box in (**c**). There is a loss in the fine structure when $\sigma > 0$, known as the bifurcation gap, and its occurrence is the basis of the modeling for dissolution of traffic congestion that we present here. See text for details.

Our traffic model makes use of a property that takes place at the noise-perturbed onset of chaos. This property is the recapitulation of the bifurcation gap. In the original studies [12], the bifurcation gap is observed by scouring the bifurcation diagram along the control parameter μ as in Figure 2. But, most remarkably, this behavior is recapitulated by the trajectories at the noise-perturbed onset of chaos [13]. It is now observed dynamically along the iteration time t for fixed $\lambda(N(\sigma)) = 0$. It manifests as two different regimes separated by a crossover from one to the other at time $t_{cross}(\sigma)$. The regime at earlier times is dynamically equivalent to the trajectories in the absence of noise: intended and systematic. In contrast, it is erratic and chaotic for later times [13]. The model for vehicular traffic is constructed and based on this recapitulation, where specific elements, trajectory

position subsequences, extracted from the mentioned full trajectories, are visualized as those of vehicles in a multilane road. More realistically, for classical vehicle positions representation, as we see below, we use the logarithm of the absolute value of trajectory positions. The earlier regular regime characterizes jam-packed traffic, while the later chaotic one represents unclogged and cleared traffic. The crossover time $t_{cross}(\sigma)$ measures the duration of traffic congestion. Or, more realistically, for classical vehicle representation, as we see below, we use its logarithm $\tau_{cross}(\sigma) = \ln t_{cross}(\sigma)$.

Interestingly, we have made earlier use of the recapitulation at the onset of chaos of the bifurcation gap to detail its analogy with glassy dynamics in molecular fluids; see [13] and ref. [5] therein. This analogy comprises four main properties observed in the formation of molecular glasses: (i) plateau interrupted relaxation, as observed in scattering experiments; (ii) Adam–Gibbs empirical law, which is a connection between relaxation times and configurational entropy; (iii) aging, as observed in the scaling of two-time correlations; (iv) diffusion arrest, which is the gradual decrement and disappearance of normal diffusion; see, for example, refs. [14–16] for documentation and description of these four leading properties of glassy dynamics.

The analysis of our model consists of the consideration of these four properties of the recapitulation of the bifurcation gap in the language of vehicular traffic; that is, we obtain a translation of the main features of glass formation into vehicular traffic terms. Analogies between these two areas of study have been indicated before [17,18], but, also, the present study constitutes a working link between nonlinear dynamics and vehicular traffic. Likewise, the correspondence between nonlinear chaotic behavior and vehicular traffic has been reported [19,20]. Therefore, this research links the three areas of study: nonlinear dynamics, glassy dynamics and vehicular traffic dynamics. We discuss our results.

2. Logistic Map with and Without Additive Noise

The trajectories of the logistic map with additive noise, as we choose to define them here, are given by.

$$x_{t+1} = 1 - \mu x_t^2 + \sigma\xi_t, -1 \leq x_t \leq 1, t = 0, 1, 2, 3, \ldots, 0 \leq \mu \leq 2, \quad (1)$$

where x_t is a trajectory position at iteration time t with initial position x_0, μ is the control parameter, $\sigma > 0$ is the noise amplitude, and ξ_t is Gaussian white noise.

2.1. Bifurcation Gap

The bifurcation diagram of the noiseless logistic map ($\sigma = 0$ in Equation (1)) is shown in Figure 2a. It is a multi-fractal set where all of its features, including the period-doubling transition to chaos (the common accumulation point already described) appears an infinite number of times at an infinite number of scales. Once $\sigma > 0$, this feature disappears and there is a bifurcation gap, at which a maximum period $2^{N(\sigma)}$ regular attractor becomes a maximum $2^{N(\sigma)}$ multi-band chaotic attractor [12] with $\lambda(N(\sigma)) = 0$. All periodic attractors and all multi-band chaotic attractors with periods or numbers of bands larger than $2^{N(\sigma)}$ are absent. Compare Figure 2b with Figure 2c. The noise fluctuations wipe out the fine structure of the bifurcation diagram. However, the gap displays scaling features similar to those in the neighborhood of a thermodynamic critical point; for instance, the shift of the control parameter value at the transition to chaos due to the noise amplitude $\Delta\mu_c \equiv \mu_c(0) - \mu_c(\sigma)$ obeys the power law $\Delta\mu_c = \sigma^\gamma$, where the value of γ is given and understood in terms of universal constants [12].

2.2. Recapitulation at the Noiseless Onset of Chaos

We look first at recapitulation at the onset of chaos of the period-doubling cascade in the absence of noise $\mu = \mu_c(0)$. In Figure 3a, we show the period-doubling cascade, the left-hand side of the logistic map bifurcation diagram, in an unusual manner: in logarithmic scales. The filled circles in this figure are the positions of the periodic supercycles or superstable attractors that have also the onset of chaos as their accumulation point [8]. The supercycles as obtained from Equation (1) with $\sigma = 0$ have always as positions $x = 0$ and $x = 1$. Notice that all supercycle positions fall along the indicated dashed diagonal lines; that is, those positions along one diagonal follow power-law scaling. In Figure 3b, we plot, also in logarithmic scales, the trajectory initiated at $x_0 = 0$ for $\mu_c(0)$, that is, at the transition to chaos. The trajectory positions, shown as filled circles, recapitulate the period-doubling cascade. Notice that these positions fall along the indicated dashed diagonal lines; that is, they follow power-law scaling. The highlighted positions in Figure 3a fall along vertical lines as they belong to periodic attractors at fixed control parameter values $\mu_n(0)$, whereas those highlighted in Figure 2b do advance along the iteration time values because the period is infinite at the accumulation point $\mu_c(0)$. Nevertheless, the trajectory in Figure 3b mimics all periods, increasing its accuracy as the iteration time increases. The positions in the first diagonal in Figure 3b progressively approach the value of the position $x = 0$ of the supercycles that is not visible in Figure 3a because of the logarithmic scales.

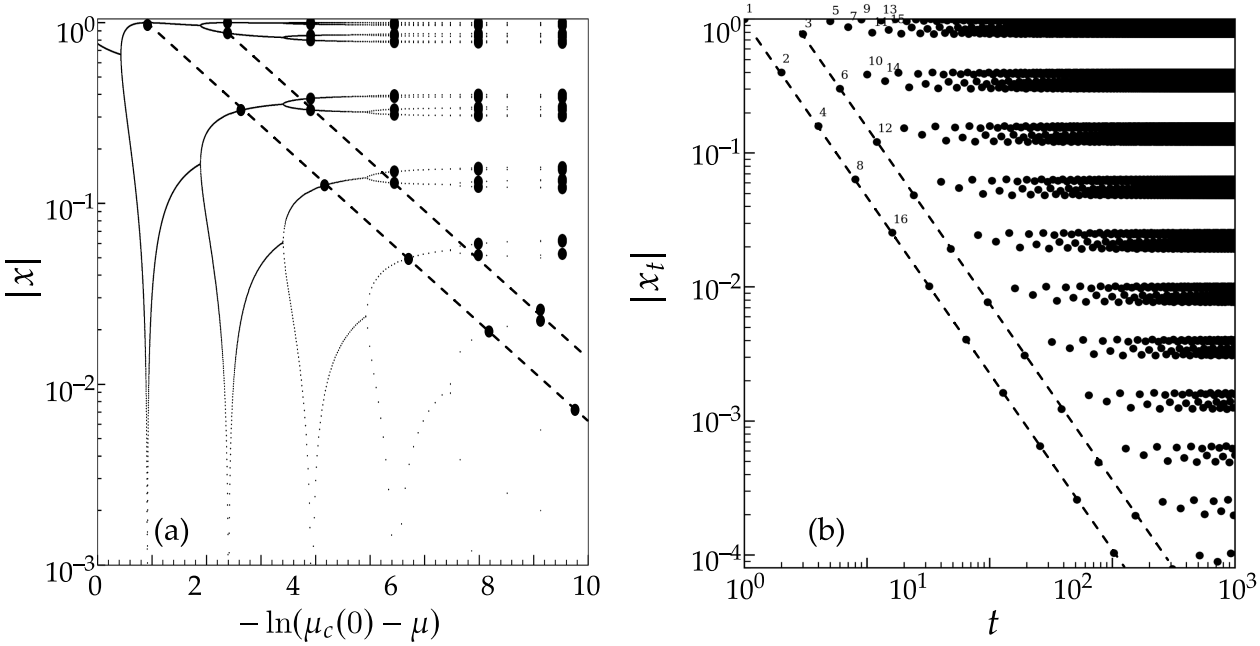


Figure 3. (**a**) A portion of the period-doubling cascade of attractors of the (noiseless) logistic map in Equation (1) with $\sigma = 0$ in logarithmic scales and absolute values of positions. The solid dots correspond to the positions of the supercycle attractors [8]. (**b**) Trajectory (initiated at $x_0 = 0$) at the period-doubling transition to chaos ($\mu_c(\sigma = 0)$ and $\lambda_{\mu_c} = 0$) for the same (noiseless) logistic map in logarithmic scales. The numbers refer to iteration times. Notice the similarities between the two panels: positions are grouped into bands and subsets of them appear aligned into same-slope diagonals. We refer to the trajectory pattern in (**b**) as recapitulation of the period-doubling cascade in (**a**). See text for details.

An interesting property of Figure 3b is that it was obtained to show the positions of a single trajectory that was initiated at $x_0 = 0$ for $\mu_c(0)$. But, it also shows all possible trajectories, an infinite number of them, that are initiated within the attractor at $\mu_c(0)$. This attractor is a multi-fractal set whose elements are the positions shown (partially and only in

absolute values) in Figure 3b. The initial position of any other trajectory within the attractor is a position x_t of the trajectory for $x_0 = 0$, and that trajectory moves in Figure 3b towards the right, progressively occupying the positions shown by circles. Actually, Figure 2b can be seen as the entire, infinite ensemble of trajectories that can be initiated within the attractor at the transition to chaos, each circle being a different possible initial position, and as the iteration time proceeds, these trajectories advance towards the right of the figure, leaving the position to be occupied by the adjacent trajectory at its left empty. All trajectories in the ensemble advance in a concerted manner. Of course, there are other trajectories that are initiated outside the attractor: the complement set of the multi-fractal set that form the real number dominion of the map, $-1 \leq x_t \leq 1$. These trajectories evolve towards and are captured by the multi-fractal attractor described.

2.3. Analytical Expressions for Position Subsequences

Yet another remarkable property of the trajectories shown in Figure 3b appears when considering the subsequences of positions that appear in the figure aligned as decreasing lines with equal slope: the diagonals referred-to above. These position subsequences can be obtained in closed analytical form [21] and several important dynamical properties associated with them can be derived exactly. These dynamical properties are of fundamental nonlinear-dynamical interest, as they reveal the universal scaling properties of the so-called renormalization group (RG) fixed-point maps $f^*(x)$ that govern all the routes to chaos in one-dimensional nonlinear maps; see [8,21]. Here, we only present, describe, and indicate how to obtain the relevant expressions, as they will be used in the formulation of the traffic model.

The position subsequences that form each of the diagonals (the entire set of positions in Figure 3b grouped into diagonals) obey the expression [21]

$$x_t = x_{t_w} \exp_q(-|x_{t_w}|^{q-1} u t/t_w), \tag{2}$$

where $\exp_q(x) \equiv [1 + (1-q)x]^{1/(1-q)}$, $t/t_w = 2^k, k = 0, 1, 2, \ldots$, $t_w = 2l + 1, l = 0, 1, 2, \ldots$, $q = 1 + \ln 2 / \ln \alpha_F$, $u = [(q-1)x_{t_w}^{(q-1)}]^{-1}$ and $\alpha_F = 2.50290\ldots$ is the absolute value of the Feigenbaum constant, the universal scaling factor for this route to chaos [8]. The positions of each diagonal subsequence in Figure 3b conforms (progressively with increasing number of iterations) with the exponential form $\alpha_F^{-k}, k = 0, 1, 2, \ldots$, and Equation (2) can be easily corroborated to reduce to $x_t/x_{t_w} = \alpha_F^{-k}, k = 0, 1, 2, \ldots$, where x_{t_w} is the initial position of each diagonal (top right position in Figure 3b).

The positions along the diagonals given by Equation (2) can be obtained from the map $f^*(x) = x \exp_q(u|x|^{q-1})$, because all of its trajectories are given by $x_{\bar{t}} = x_0 \exp_q(|x_0|^{q-1} u \bar{t})$, $\bar{t} = 0, 1, 2, \ldots$, and these trajectories can in turn be transformed into those given by Equation (2) with the use of $\bar{t} = t/t_w$ and the previous definitions given above for q and u. The map $f^*(x)$ is the RG fixed-point map for the most tractable route to chaos (via the tangent bifurcation [8]) whereas the RG fixed-point map trajectories for the period-doubling route to chaos can be assembled analytically via Equation (2) [21]. These trajectories have scaling properties that all unimodal quadratic maps (including the logistic map) obey asymptotically with an increasing number of iterations. In Figure 4a, we show a few trajectories of the RG fixed-point map $f^*(x) = x \exp_q(u|x|^{q-1})$, obtained initially for consecutive values of the iteration time, but shown there with t now in the form $t/t_w = 2^k, k = 0, 1, 2 \ldots$, and in Figure 4b (in logarithmic scales) as the first few diagonals given by Equation (2).

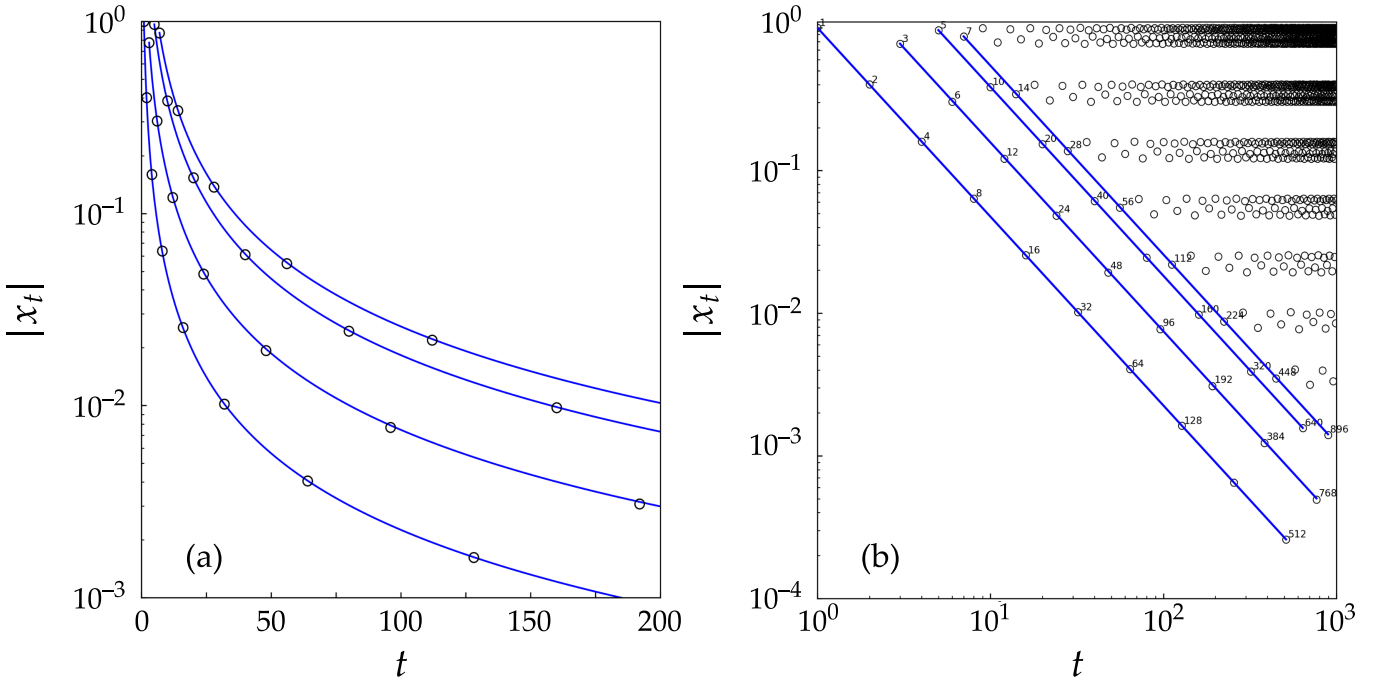


Figure 4. (**a**) Consecutive iteration time trajectories obtained from the map $f^*(x) = x \exp_q(u|x|^{q-1})$ for a fixed value of q and four different values of u and initial positions x_0 but shown for times $t = (2l+1)2^k, k = 0, 1, 2, \ldots$, with one value of $l = 0, 1, 2, 3$ for each trajectory. The values of these parameters are chosen to fulfill Equation (2) with $t_w = 1, 3, 5, 7$, and are according to the definitions given to q and u below this equation. (**b**) The same four trajectories' positions in logarithmic scales superposed on the positions of the trajectory shown in Figure 3b. The numbers refer to iteration times. Thus, each subset of positions forming diagonals can be obtained analytically from Equation (2). The multilane vehicle model makes use of these positions.

2.4. Recapitulation of the Bifurcation Gap

As already mentioned, the bifurcation gap produced by additive noise of amplitude σ is recapitulated at the transition to chaos that takes place when the Lyapunov exponent $\lambda(N(\sigma)) = 0$. The trajectory initiated at $x_0 = 0$ (or, equivalently, all the trajectories initiated at all positions of the multi-fractal attractor at the noiseless $\sigma = 0$ transition to chaos) exhibits two regimes separated by a crossover iteration time given by $t < t_{cross}(\sigma)$ [13]. For times $t < t_{cross}(\sigma)$, the trajectory, or trajectories, proceed as in the noiseless recapitulation dynamics, up to the recapitulation that approximates period $2^{N(\sigma)}$; that is, the structure of position diagonals in Figures 3b and 4b is preserved for times $t < t_{cross}(\sigma)$. But, for times $t > t_{cross}(\sigma)$, the trajectories begin to behave chaotically and the ordered pattern enters a gradual disarray. At iteration times $t < t_{cross}(\sigma)$, the precise values of the noiseless positions show small deviations due to the noise, but for times $t > t_{cross}(\sigma)$, the order in which the bands or diagonals are visited in the noiseless dynamics is broken. This is shown in the panels of Figure 5, where the noiseless positions are shown in the background and positions joined by dashed lines are shown for noisy trajectories only for selected times that correspond to the time subsequences of the first four diagonals. For clarity of presentation, each panel in Figure 5 shows noisy trajectories for different time subsequences. As the noise amplitude $\sigma \to 0$ and $t_{cross}(\sigma) \to \infty$, the concerted multiple-band and multiple-diagonal dynamical structure shown in Figures 3b and 4b is gradually recovered.

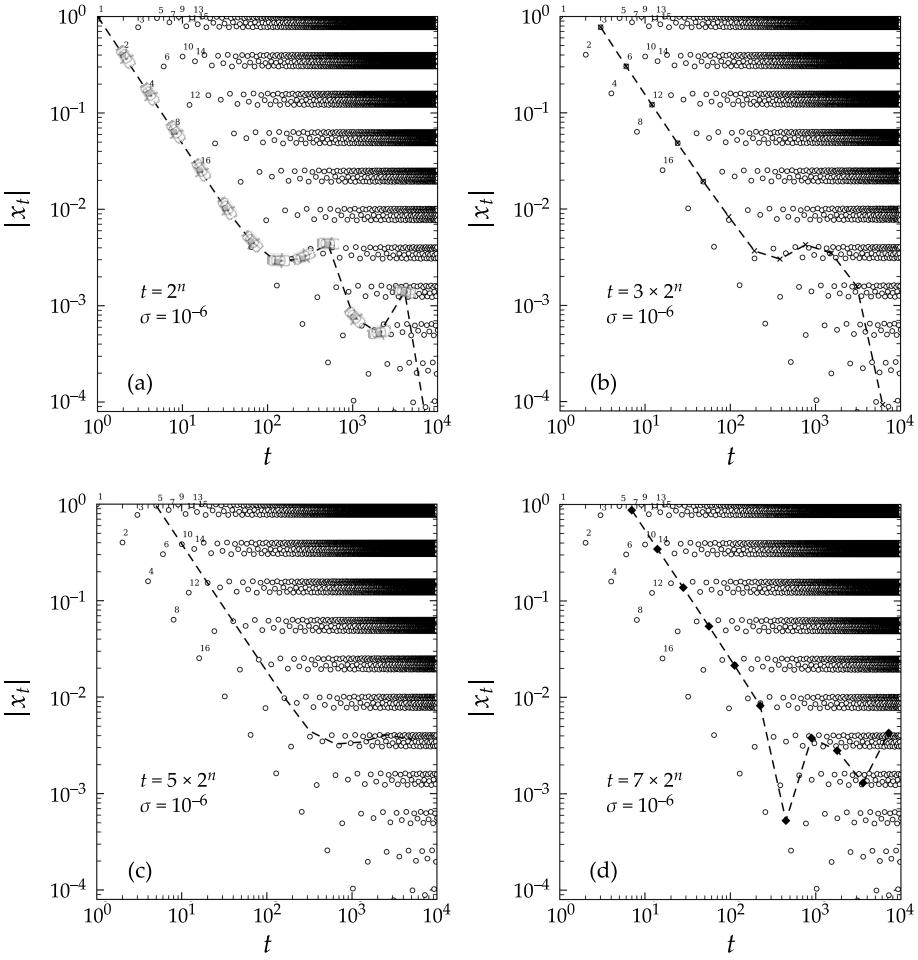


Figure 5. Absolute values of positions x_t and iterations t in logarithmic scales for various trajectories at the onset of chaos $\mu_c(\sigma)$ starting at $x_0 = 0$. Open circles correspond to the noiseless trajectory and the numbers label time $t = 1, \ldots, 16$. Dashed lines represent position trajectories for noise amplitude $\sigma = 10^{-7}$ plotted only at selected times. (**a**) $t = 2^n, n = 0, 1, 2, \ldots$. (**b**) $t = 3 \cdot 2^n, n = 0, 1, 2, \ldots$. (**c**) $t = 5 \cdot 2^n, n = 0, 1, 2, \ldots$. (**d**) $t = 7 \cdot 2^n, n = 0, 1, 2, \ldots$. As observed, there is a crossover time t_{cross} between two regimes: at times $t < t_{cross}$, the trajectories behave similarly to the noiseless case $\sigma = 0$ but at times $t > t_{cross}$, the trajectories do not and follow erratic patterns. These two regimes are used in our vehicular traffic model, where the 1st represents jammed traffic and the 2nd normal flow. The logarithm of the crossover time t_{cross} indicates the traffic jam duration, a function of noise amplitude σ.

3. Traffic Models Based on the Recapitulation of the Bifurcation Gap at the Period-Doubling Transition to Chaos

The nonlinear dynamical properties described in the previous section offer elements from which models, or rather model variants, for vehicular traffic can be constructed. We elaborate three of them here; the first two represent, in a simplified manner, the flow of a large number of vehicles on a multilane road, and can be classified as microscopic traffic models. The two models are built up by considering sets of subsequences of positions of trajectories, those we have called diagonals, generated by the logistic map at the transitions to chaos and shown in Figures 3b and 4b. The numbers of diagonals considered are all adjacent; that is, a road of L lanes is made of the first L diagonals in Figures 3b or 4b with $l = 0, 1, 2, \ldots, L - 1$, where each position of each diagonal is occupied by a vehicle in congested traffic. Realistic vehicle distances are given by the logarithm of the absolute value of these positions. The third model is different: it is a repeated-cell map [8] where

the addition of noise releases traffic into neighboring zones, operates at scales larger than vehicular sizes, and can be classified as macroscopic traffic model.

The first model variant displays two regimes: one describes congested traffic, where vehicles advance in an orderly fashion via unit vehicle length displacements and only when the front vehicle does likewise; also, vehicles cannot change lane. In the other regime, vehicles move more freely, interchange lanes, and can abandon the road, while new ones are incorporated. As we shall see later, the model also describes features of a network of multilane roads, as they exist in urban areas. Vehicle space positions on lane l, χ_{τ_l}, at time τ_l in the model are the logarithms of positions of the trajectory in the map: $\chi_{\tau_l} \equiv \ln|x_t|$ and $\tau_l \equiv \ln t = \ln(2l+1) + k\ln 2$. Notice that the time taken for a single vehicular advance is lane dependent, the fastest lane is the main diagonal and the lane average velocity decreases with l. Initially, the logistic map is tuned at the transition to chaos in the absence of noise. When $\sigma = 0$, we have fully congested traffic, where the vehicles are each confined to a lane and move only one space (next position in the subsequence) per unit time τ_l for lane l; that is, each vehicle advances one slot because the vehicle in front has done so. This regime continues until the multilane crossover times $\tau_l^*(\sigma) \approx \ln(2l+1) + N(\sigma)\ln 2, l = 0, 1, 2, \ldots, L-1$. After the crossover, the recapitulation of the bifurcation gap leads to the second regime, the dissolution of the traffic jam, where vehicles change lanes, abandon the road (as trajectories move out of the chosen first L diagonals) or enter the road (as trajectories move into the chosen first L diagonals). The length and duration of traffic congestion is a function of the applied noise amplitude σ; see Figure 5.

The second traffic model variant is also based on the same set of L diagonals and it is designed to display a specific behavior generally observed when stopped lines of vehicles start to advance, say, when the traffic light releases movement. To this purpose, we make use of trajectories at the onset of chaos in the absence of additive noise $\sigma = 0$ and the fact that these trajectories have infinite memory, so that they can be reversed in time. We use the diagonal positions x_t of the trajectory initiated at $x_0 = 0$ in Equation (2). We consider this trajectory until it reaches a chosen position, say x_M, M large. We recall that this set of positions can also be seen as the positions of M trajectories with initial positions from $x_0 = 0$ to $x_0 = x_M$. In other words, this is equivalent to having L diagonal segments filled with vehicles; see Figure 6. If the trajectory is reversed in time, starting at $x_0 = x_M$ now ends at $x_M = 0$, and the L diagonal segments of the multilane road are transversed by the packed vehicles in the opposite sense. Suppose now that a traffic light at $x = 0$ releases traffic movement, the first vehicle in diagonal l moves at time $2l+1$, the second at time $(2l+1)2$, and so on, and the k-th vehicle moves at time $(2l+1)2^k$. This is analogous to the time delay along the queue line after traffic release, as observed for vehicle advances in congested lanes.

A third traffic model variant is built by the use of the logistic map at the transition to chaos ($\mu = \mu_c(0)$) as the element of a repeated-cell map [8] in such a way that additive noise leads to an stochastic scape rate to neighboring cells [13]. The periodic map is given by $f(x_{t+1}) = f(x_t)$, $f(m+x) = m + f(x)$, $m = \ldots, -1, 0, 1, \ldots$, where

$$f(x) = \begin{cases} -|1 - \mu_c x^2| + \sigma\xi, & -1 \le x < 0 \\ |1 - \mu_c x^2| + \sigma\xi, & 0 \le x < 1. \end{cases} \tag{3}$$

See Figure 7, where it can be noticed that the quadratic map has been split into two mirror image segments to form the map for each cell. Notice too that the minimum and the maximum of the map in each cell touch the square cell top and bottom. In the absence of noise, all trajectories remain in the cell where they are initiated. The addition

of noise allows for sporadic scape of trajectories to the neighboring left and right cells. If the random variable term at iteration time t overcomes the cell extremum, the trajectory escapes to the neighboring cell; otherwise, it remains confined. This model construction allows one to retain trajectories, in our case, vehicles, in a single cell, or location or urban region, or the opposite: to promote transit across distant locations (cells) as a function of the noise amplitude σ.

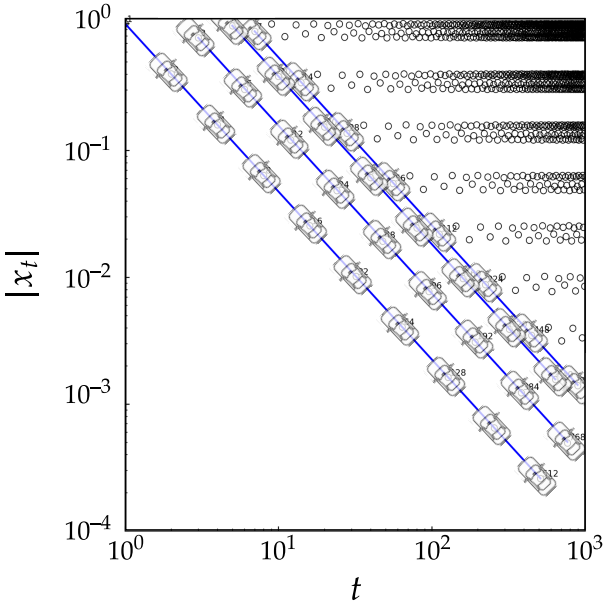


Figure 6. The trajectory positions in Figure 4b are reproduced to define a model variant for vehicular traffic. A multilane road is formed by the 1st L diagonals, $L = 4$ in the figure. Each lane position is occupied by a vehicle, each of which advances to the next position towards the left upper corner. Lane unit distance is measured by $\Delta\chi \equiv \chi_{t+1} - \chi_t = \ln|x_{t+1}| - \ln|x_t|$ and the k-th vehicle on line $l = 0, 1, 2, 3$ moves at time $(2l+1)2^k, k = 0, 1, 2, \ldots$. Vehicles take increasingly longer times to advance a unit position the farther their queue line positions from the beginning of the lane. See text.

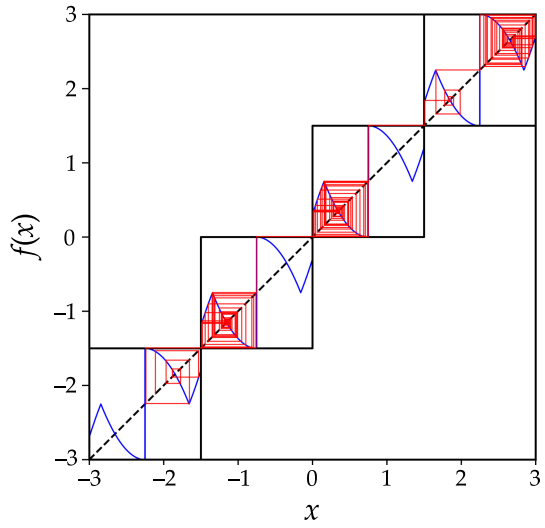


Figure 7. Another variant for vehicular traffic defined via a repeated-cell map. The map for each cell (shown in blue) is given by Equation (3). The trajectories (shown in red) can migrate to neighboring cells when the trajectory position is near the top or bottom of a cell and the additive noise random value allows the trajectory position to exceed the cell boundaries. The model permits the evaluation of the mean-square displacement of vehicles diffusing throughout neighborhoods represented by the cells. See text.

Summary of the three model variants:

- In the first model variant, we select position subsequences that we call diagonals (shown in Figure 4b) from the full map trajectory to design a multilane road for vehicular traffic. The chosen trajectory (absolute value) positions at their iteration times $|x_t|$ are converted into vehicular positions and advancement times by taking their logarithms since vehicles then become equally spaced and advance at equal time intervals to adjacent positions, as in slow flow traffic.
- In the second model variant, we set the noise amplitude equal to zero $\sigma = 0$ and make use of the same diagonal position subsequences as above but we first reverse the traffic direction (as shown in Figure 6). We use again the logarithm of the (absolute value) of trajectory positions $|x_t|$ as vehicle positions, but leave the iteration times as vehicle times for advancement. In this way, this variant models the increasing (power-law) time delay for vehicular advancements along the queue line when congested traffic allows movement.
- In the third model variant, we aim to describe vehicular traffic at large scale across a sequence of urban zones. We made use of a repeated-cell map with logistic map single-cell features. This time, the use of noise becomes a stochastic scape rate for trajectories to neighboring cells. For large noise amplitude σ, there is free macroscopic traffic flow, but as this amplitude is made to vanish, zone entrapment develops and finally blocks neighborhoods.

4. Parallels Between the Dynamics of Congested Traffic and Glass Formation

We describe four characteristic properties of the dynamics of glass formation and reinterpret them in the language of congested traffic and its dissolution. To do this, we make use of the model variants described in the previous section. As we have expressed, in doing this, we employ the nonlinear dynamical properties of a quadratic map at the transition to chaos with additive noise. Normally, the dynamical properties of glass formation in molecular systems are presented in terms of decreasing temperature; in our case, this is analogous to diminishing the amplitude σ of the applied noise. Naturally, in our nonlinear dynamical modeling, the breakup and disbandment of congested traffic are obtained in the opposite manner: increasing σ.

4.1. Plateau Interrupted Relaxation

A two-step relaxation process is observed in the equilibrium two-time correlations in supercooled liquids as they approach glass formation. There are two power-law decays in the correlations separated by a plateau of constant correlation. The first decay is named ballistic [14,22] as when molecules appear to move unencumbered at short correlation times. The plateau is identified with a time interval that increases as temperature decreases, in which molecules are caged by their neighbors [14]. The second decay signals molecular group motions that break the caged regime. The correlations that display this behavior comply with time translation invariance $t = t_2 - t_1$, so they effectively depend on only one time variable and are considered to be equilibrium or thermalized correlations. This behavior is captured by the dynamics of trajectories at the logistic map with additive noise that take place at $\mu_c(\sigma)$ when $\lambda(\mu_c(\sigma)) = 0$ [13]. The correlation function for these trajectories is given by

$$c_e(t_1, t_2) \equiv \frac{\langle x_{t_2} x_{t_1} \rangle - \langle x_{t_2} \rangle \langle x_{t_1} \rangle}{\langle \bar{x}_{t_1} \bar{x}_{t_2} \rangle}, 1 \leq t_1 \leq t_2, \tag{4}$$

where $\bar{x}_{t_i} \equiv \sqrt{\langle x_{t_i}^2 \rangle - \langle x_{t_i} \rangle^2}, i = 1, 2$, and $\langle \dots \rangle$ represents an average over an ensemble of trajectories started at $x_0 = 0$ [13]. It was found that $c_e(t_1, t_2) \simeq c_e(t)$, $t = t_2 - t_1$, t_1 large [13].

The first power-law decay is observed only if the trajectory is initiated outside the attractor (the analog of the early ballistic regime), the plateau corresponds to the bifurcation gap recapitulation regime $t < t_{cross}(\sigma)$, and the second power-law decay takes place during the bifurcation gap recapitulation second regime $t > t_{cross}(\sigma)$ [13]; see Figure 8. In the multilane road traffic model, the first decay corresponds to the approach of the congested road, the plateau is congested traffic, and the second decay is the dissolution of the traffic jam. The traffic jam duration is given by $t_{cross}(\sigma)$.

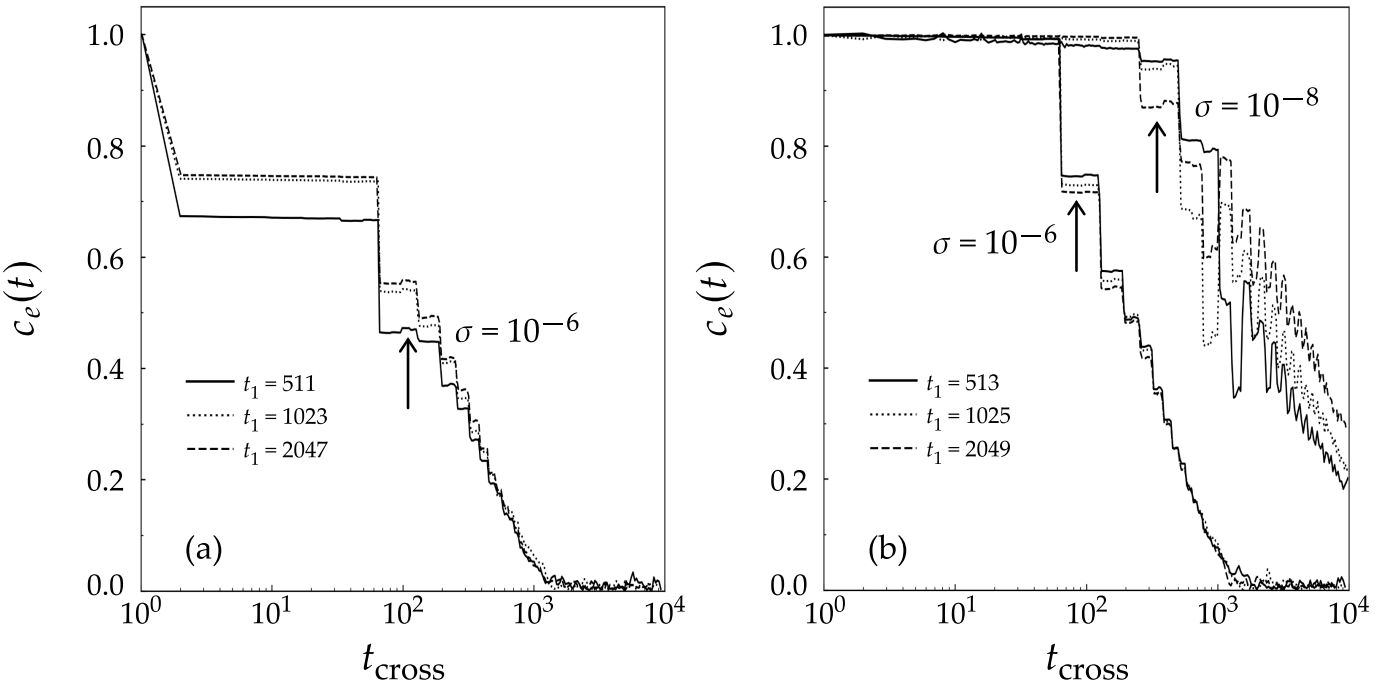


Figure 8. Relaxation at the onset of chaos according to the correlation function $c_e(t), t = t_2 - t_1$ defined in Equation (4) for an ensemble of 300 trajectories starting at $x_0 = 0$. In (**a**), $t_1 = 2^n - 1$ and the noise amplitude is $\sigma = 10^{-6}$. In (**b**), $t_1 = 2^n + 1$ and the noise amplitude is $\sigma = 10^{-6}$ and $\sigma = 10^{-8}$. Vertical arrows indicate the crossover time t_{cross}. For the vehicular traffic model, the constant correlation plateau corresponds to the traffic jam where any vehicle can only move when the vehicle in front moves. The correlation decay for $t > t_{cross}$ indicates increasing independence of vehicle advances.

4.2. Relaxation Times and Configurational Entropy

An inverse exponential relationship between relaxation times and configurational entropy has been documented from observations of molecular glassy dynamics [14]. Relaxation time diverges and entropy vanishes as temperature approaches the vitreous state. This is known as Adam–Gibbs law [14] and links dynamics with thermodynamics. Again, this property is captured by the dynamics of trajectories at the logistic map with additive noise that take place at $\mu_c(\sigma)$ when $\lambda(\mu_c(\sigma)) = 0$ [13], a difference being that we obtain a power law instead of an exponential law because we restrict our calculations to the onset of chaos [13], and this transforms exponential decay into power-law decay as it is the case in critical point phenomena. Briefly, at the crossover iteration time $t_{cross}(\sigma) = 2^{N(\sigma)} = \sigma^{r-1}$,

$r - 1 \simeq -0.3668$ [13], the entropy S_c of the $2^{N(\sigma)}$ band attractor is $S_c = 2^{N(\sigma)}\sigma s$, where s is the entropy (per unit amplitude σ) of a single noise-generated band. One obtains

$$t_{cross} = (s/S_c)^{(1-r)/r}, \tag{5}$$

and we have $t_{cross} \to \infty$ and $S_c \to 0$ as $\sigma \to 0$. As we have concluded in the multilane road traffic model, $t_{cross}(\sigma)$ is the traffic jam duration, and therefore S_c could be interpreted as an entropy associated with vehicle maneuverability options. This complies with the limits associated with $\sigma \to 0$, compatible with the first regime $t < t_{cross}(\sigma)$ of the bifurcation gap recapitulation as well as with its second regime $t > t_{cross}(\sigma)$ when the effect of the noise amplitude becomes explicit; see Figure 9.

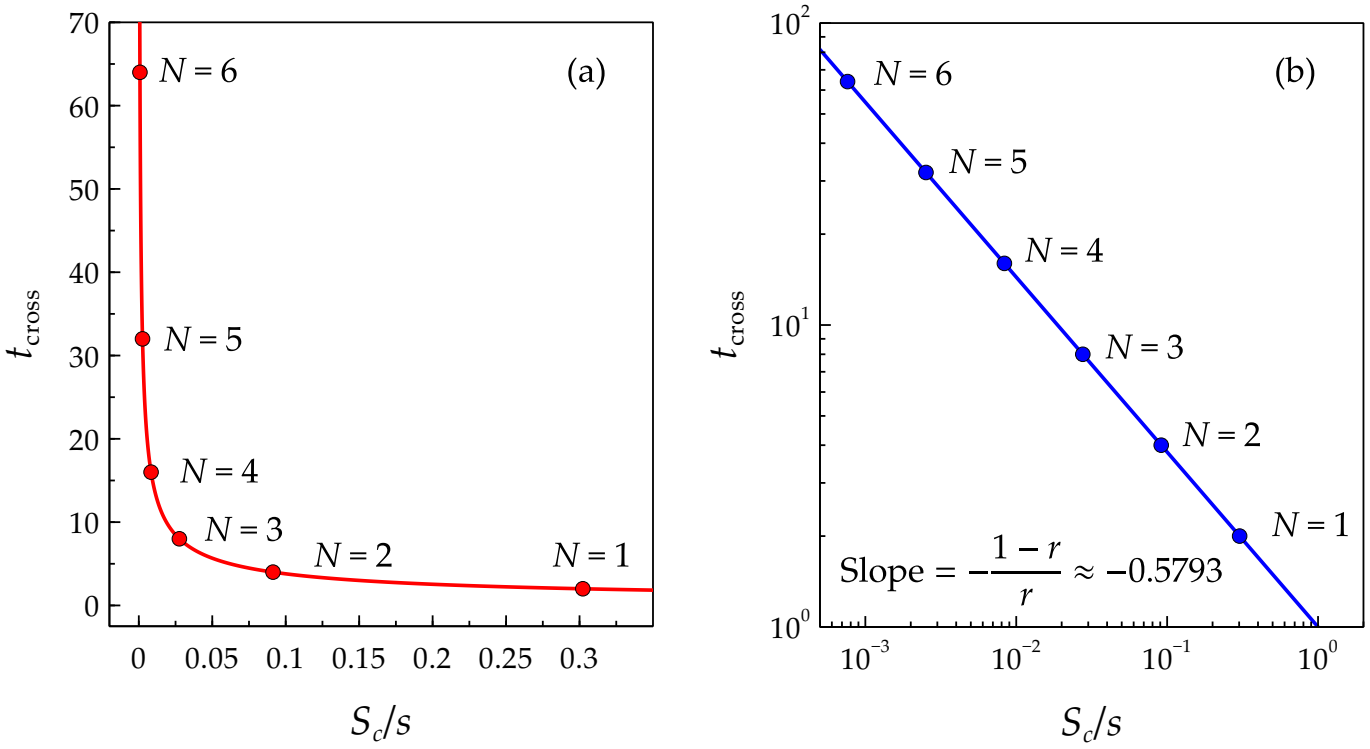


Figure 9. Crossover time t_{cross} displayed by trajectories at the noise-perturbed transition to chaos as a function of configurational entropy S_c/s as given by Equation (5), (**a**) ordinary scales and (**b**) logarithmic scales. The numbers N correspond to the maximum allowed recapitulation of periods $1, 2, 4, 8, \ldots, 2^N$ before the outbreak of chaotic dynamics. In glassy dynamics, this law indicates that the relaxation time to equilibrium increases as the molecular configurations become more obstructed. In the traffic model, it indicates that the duration of traffic jams increases as vehicular maneuvers become more restricted; see text.

4.3. Aging

As temperature closes into the vitreous state, time translation invariance breaks down in the two-time correlations of glass formers (as mentioned, in equilibrium liquid states, they normally depend only on $t \equiv t_2 - t_1$). Interestingly, correlations in this different regime display scaling with the time-ratio variable $\bar{t} = t/t_w$, known as aging, where $t_1 \equiv t_w$ and t_w is commonly named as waiting time [14]. The equivalent phenomenon is captured by the correlation function of trajectories of the logistic map at the onset of chaos with additive noise. Aging is displayed in the first regime of the recapitulation of the bifurcation gap, $t < t_{cross}(\sigma)$. As we have seen, this regime is dynamically similar to the noiseless recapitulation at the onset of chaos. And the latter, as opposed to chaotic

dynamics, is nonergodic [13]. Therefore, we do not consider ensemble averages, like in Equation (4), to define the correlation function in this regime. Instead, we define it as [13]

$$c(t, t_w) \equiv \sum_{n=n_0}^{N} \phi^{(n)}(t_w)\phi^{(n)}(t_w + t), \tag{6}$$

where $\phi(t) = f_{\mu_c}^{(t)}(0)$, $n_0 = 1, 2, 3, \ldots$ and $N \gg n_0$. The results are shown in Figure 10a and the waiting time scaling (collapse by shifts in logarithmic scales into a single curve) is demonstrated in Figure 10b. Aging in the multilane traffic model in its congested state ($t < t_{cross}(\sigma)$) corresponds to the different vehicle speed for each lane $l = 0, 1, 2, \ldots, L-1$ as imposed by the iteration time factor $t_w = 2l + 1$. Aging also appears, but in a different way, in the second traffic model illustrated in Figure 6.

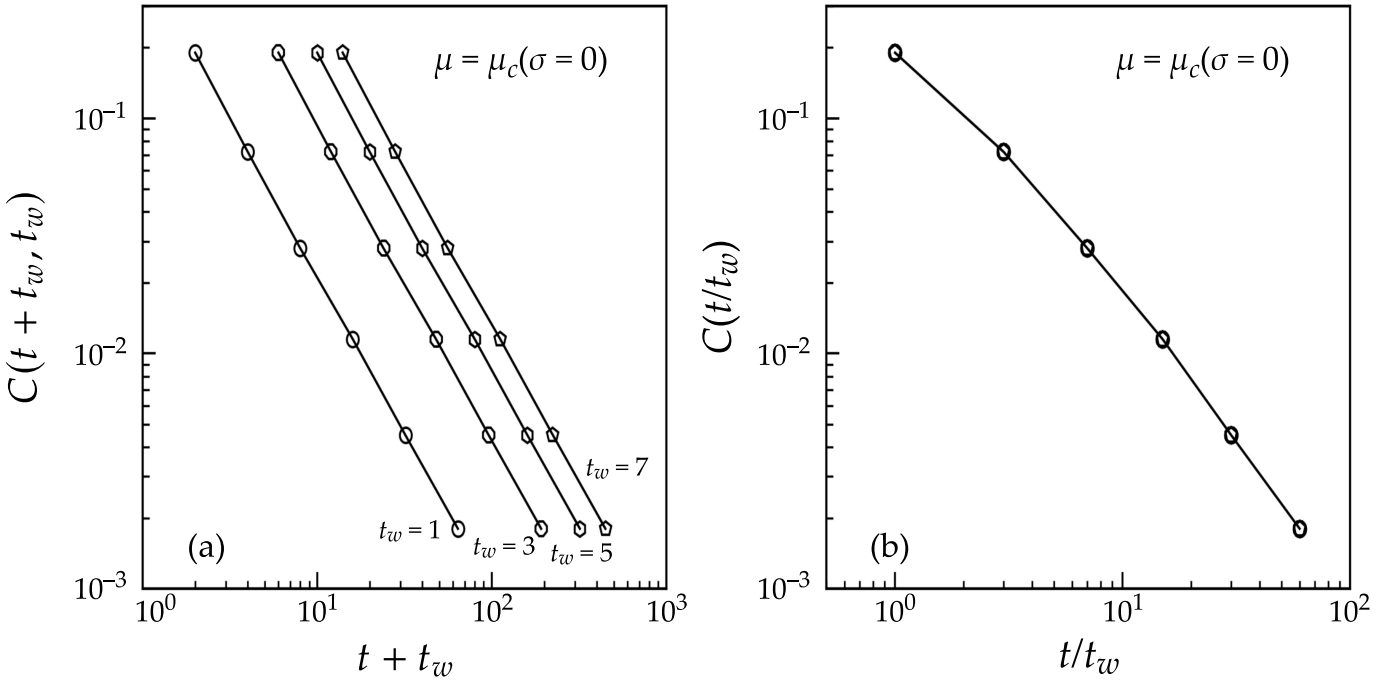


Figure 10. Aging in the two-time correlation Equation (6). With additive noise, this is observed in the regime $t < t_{cross}$ as well as in the noiseless case. In (**a**), we show the correlation $c(t, t_w)$ as a function of $t + t_w$ for several values of t_w. Clearly, the decay of the correlation depends on the waiting time t_w. In (**b**), we show how these correlations collapse into a single curve upon rescaling t/t_w. Aging is observed in congested traffic as all vehicle movements are necessarily coordinated with others; see text.

4.4. Diffusion Arrest

Another manifestation of the approach of vitrification in molecular liquids is the gradual but inevitable suppression of diffusiveness, from normal diffusion to total arrest, as illustrated by the slower linear growth with time to a final halt of the molecular mean-square displacement as the temperature decreases in supercooled liquids [14]. This decline in the molecular dynamics is caused by confinement, where molecules become trapped by their own neighbors, and individual releases or collective rearrangements require coordinated motions of increasing numbers of them as the temperature is lowered. Our repeated-cell map described in the previous section provides ensembles of trajectories from which the mean-square displacement can be obtained as a function of the noise amplitude σ. This is shown in Figure 11, where we can observe the progression from normal diffusiveness to a total halt and entrapment within single map cells as the noise is removed. In terms of our third traffic model, the decline in diffusion as measured by

that of the mean-square displacement of ensembles of trajectories that spread across the repeated-cell map indicates vehicular entrapment in urban zones or districts defined by the map cells. The model describes vehicular clogging at larger scales.

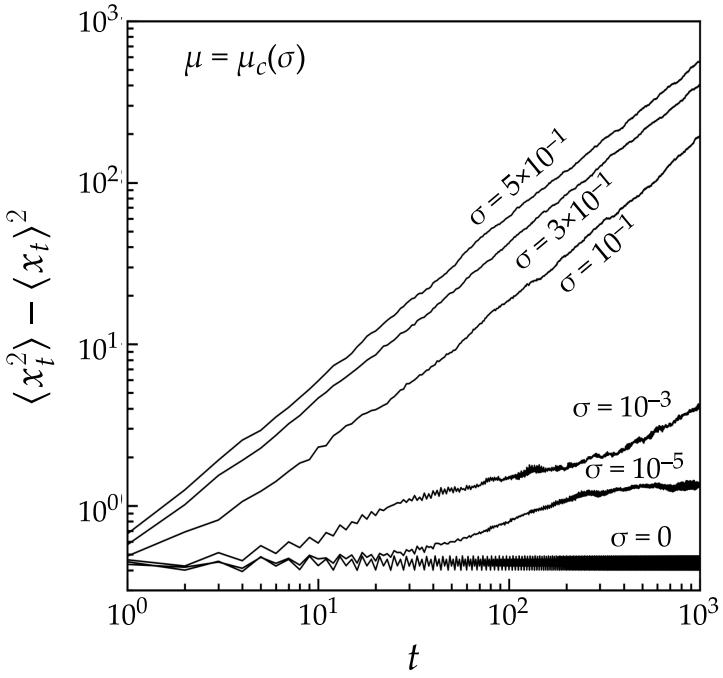


Figure 11. The mean-square displacement of trajectories that move throughout the repeated-cell map in Equation (3) and shown in Figure 7. Displacement increases linearly with iteration time t for large noise amplitude σ even of order 10^{-1}, but as this amplitude diminishes, the displacement growth decreases and eventually vanishes for $\sigma = 0$, when trajectories become trapped within a cell. In a molecular liquid, linear growth is characteristic of Brownian motion and normal diffusion, whereas near vitrification, vanishing displacement indicates diffusion arrest. For the corresponding traffic model, linear displacement growth indicates free vehicular movement across neighborhoods (cells) and displacement vanishing represents entrapment at urban zone scales (cells).

5. Summary and Discussion

We have constructed and examined in detail a nonlinear dynamical model (with variants) descriptive of jammed traffic and its breakup. The model is based on the recapitulation of the bifurcation gap that takes place in the logistic map at the noise-perturbed onset of chaos. Two variants of the model are obtained from subsets of positions of trajectories that form a multilane road where vehicles occupy these positions. Vehicular distances are measured in trajectory position logarithmic scales while the logarithm of iteration times, or, when appropriate, the iteration time itself, serves as vehicular consecutive advances. The third model variant is obtained from a repeated-cell map, where each cell contains a logistic map at the period-doubling transition to chaos and where the addition of noise allows sporadic escape of trajectories to neighboring cells, allowing for the description of traffic at larger spatial scales.

We have shown that the properties of the vehicular traffic model variants are analogous to the main features observed in the dynamics of glass formation: (i) "Bumper-to-bumper" jam-packed multilane road relates to plateau interrupted relaxation; (ii) the link between the ending of a traffic jam and access to vehicle maneuver alternatives relates to the connection between relaxation time and configurational entropy; (iii) increasing delay time for vehicular advance, the longer the queue line distance from the traffic light, relates to the aging scaling property of two-time correlations; (iv) transit through increasingly

congested urban zones relates to diffusion arrest. These parallel behaviors are visualized when decreasing the noise amplitude is considered similar to reducing temperature.

The replacement via a noise source of the vastly interconnected interactions of many degrees of freedom in molecular fluids is, historically and nowadays, a surprisingly successful simplification known as Langevin theory [23]. In the same way, the effect of external noise in one-dimensional nonlinear maps can be thought to represent the interplay of many other identical systems coupled to it, like in the so-called coupled map lattices [24]. This drastic replacement was considered to be the underlying reason for the parallels found earlier [13] between the dynamics at the noise-perturbed onset of chaos in logistic maps and the dynamics of glass formation. Furthermore, the numerical study of asynchronous coupled logistic maps [25] has revealed that the properties of many interconnected logistic maps are difficult to distinguish from those of the single logistic map with additive noise, as considered here. In terms of our interest in vehicular traffic modeling, and in the same spirit as in Langevin theory, urban interconnected multilane road networks are well represented by our use of the effect of noise on a vehicle-congested single multilane road. Therefore, it is of interest to study the counterpart of the recapitulation of the bifurcation gap at the period-doubling onset of chaos in asynchronous coupled logistic maps.

Since we have here identified analogous behaviors between glassy dynamics and vehicular traffic dynamics, precisely when described via nonlinear dynamics, we cite the much debated, still-hypothetical, ideal glass [26]. In terms of our vehicular traffic model, the ideal glass is represented by vehicles occupying all the infinite subsequence sets of diagonal positions in the absence of noise, or $\tau_{cross} \to \infty$.

Finally, a concise summary:

- Our main objective, to establish an analogy between the dynamical properties of glass formation and the dissolution of congested vehicle traffic, was accomplished.
- We made use of the recapitulation of the bifurcation gap at the onset of chaos, a nonlinear dynamical property, to construct a basic multilane road model for vehicular traffic with three variants: two for microscopic and one for macroscopic traffic. The latter considers diffusion rather than fluid flow.
- The main feature of the model is a crossover time τ_{cross}. It describes jammed traffic for $\tau < \tau_{cross}$, start of jam dissolution at $\tau = \tau_{cross}$, and free traffic flow for $\tau > \tau_{cross}$.
- Four essential properties of glassy dynamics—(i) plateau interrupted relaxation; (ii) aging time correlations; (iii) relationship between relaxation time and configurational entropy; and (iv) diffusion arrest—were identified in the traffic model. In the same order: (i) locked up vehicular advancement; (ii) increasing time gap for vehicular initial advancement down queue line position; (iii) size and duration of traffic jams increases as vehicular maneuvers become restricted; (iv) vehicular clogging of urban zones obstructs large-scale displacements.
- The model traffic jam duration τ_{cross} increases as the noise amplitude decreases. The noise amplitude in the traffic model was found to measure a lack of large-scale road alternatives, since coupled maps, equivalent to road networks, behave as a single map with additive noise. In glassy dynamics, the noise amplitude measures temperature, the increment of which favors fluidity.

Author Contributions: Conceptualization, S.E.T.-F. and A.R.; methodology, S.E.T.-F. and A.R.; software, S.E.T.-F.; validation, S.E.T.-F. and A.R.; formal analysis, S.E.T.-F. and A.R.; investigation, S.E.T.-F. and A.R.; resources, S.E.T.-F. and A.R.; writing—original draft preparation, A.R.; writing—review and editing, A.R.; visualization, S.E.T.-F.; supervision, A.R.; project administration, A.R. All authors have read and agreed to the published version of the manuscript.

Funding: This research was funded by Universidad Nacional Autónoma de México, IN106625-PAPIIT-DGAPA-UNAM.

Institutional Review Board Statement: Not applicable.

Informed Consent Statement: Not applicable.

Data Availability Statement: No new data were created or analyzed in this study. Data sharing is not applicable to this article.

Conflicts of Interest: The authors declare no conflicts of interest.

References

1. Traffic Congestion, Wikipedia. Available online: https://en.wikipedia.org/wiki/Traffic_congestion (accessed on 2 August 2026).
2. Kumar, M.; Kumar, K.; Das, P. Study on road traffic congestion: A review . *Int. J. Syst. Assur. Eng. Manag.* **2021**, *12*, 976–998. [CrossRef]
3. Robledo, A. From statistical mechanics to nonlinear dynamics and into complex systems. *Complexities* **2026**, *2*, 3. [CrossRef]
4. Fosu, G.O.; Agyemang, O. Review of microscopic traffic flow models: Historical developments and future trends. *Eng. Appl. Sci. Lett.* **2025**, *8*, 29–49. [CrossRef]
5. Maslow, E. A literature review of microscopic traffic flow models: Modern and future. *Sci. Prepr.* **2025**. [CrossRef]
6. Mohan, R.; Ramadurai, G. State-of-the-art of macroscopic traffic flow modelling. *Int. J. Adv. Eng. Sci. Appl. Math.* **2013**, *5*, 158–176. [CrossRef]
7. Zhang, L.; Yuan, L.; Yang; L. Liu, Z. Recent developments in traffic flow modeling using macroscopic fundamental diagram. *Transp. Rev.* **2020**, *40*, 689–710. [CrossRef]
8. Schuster, H.G. *Deterministic Chaos. An Introduction*, 2nd ed.; VCH Publishers: Weinheim, Germany, 1988.
9. Beck, C.; Schlogl, F. *Thermodynamics of Chaotic Systems*; Cambridge University Press: Cambridge, UK, 1993.
10. Hilborn, R. *Chaos and Nonlinear Dynamics*, 2nd ed.; Oxford University Press: New York, NY, USA, 2000.
11. Logistic Map, Wikipedia. Available online: https://en.wikipedia.org/wiki/Logistic_map (accessed on 2 August 2026).
12. Crutchfield, J.P.; Farmer, J.D.; Huberman, B.A. Fluctuations and simple chaotic dynamics. *Phys. Rep.* **1982**, *92*, 45. [CrossRef]
13. Baldovin, F.; Robledo, A. Parallels between the dynamics at the noise-perturbed onset of chaos in logistic maps and the dynamics of glass formation. *Phys. Rev. E* **2005**, *72*, 066213. [CrossRef] [PubMed]
14. De Benedetti, P.G.; Stillinger, F.H. Supercooled liquids and the glass transition. *Nature* **2001**, *410*, 259. [CrossRef] [PubMed]
15. Angell, C.A.; Ngai, K.L.; McKenna, G.B.; McMillan, P.F.; Martin, S.W. Relaxation in glassforming liquids and amorphous solids. *J. Appl. Phys.* **2000**, *88*, 3113. [CrossRef]
16. Berthier, L.; Biroli, G. Theoretical perspective on the glass transition and amorphous materials. *Rev. Mod. Phys.* **2011**, *83*, 587–645. [CrossRef]
17. de Wijn, A.; Miedema, D.; Nienhuis, B.; Schall, P. Criticality in dynamic arrest: Correspondence between glasses and traffic. *Phys. Rev. Lett.* **2012**, *109*, 228001. [CrossRef] [PubMed]
18. Gravish, N.; Gold, G.; Zangwill, A.; Goodisman, M.; Goldman, D. Glass-like dynamics in confined and congested ant traffic. *Soft Matter* **2015**, *11*, 6552. [CrossRef] [PubMed]
19. Li, T. Nonlinear dynamics of traffic jams. *Phys. D. Nonlinear Phenom.* **2005**, *207*, 41–51. [CrossRef]
20. Orosz, G.; Wilson, R.; Szalai, R.; Stepan, G. Exciting Traffic Jams: Nonlinear Phenomena Behind Traffic Jam Formation on Highways. *Phys. Rev. E* **2009**, *80*, 046205. [CrossRef] [PubMed]
21. Robledo, A.; Velarde, C. How, why and when Tsallis statistical mechanics provides precise descriptions of natural phenomena. *Entropy* **2022**, *24*, 1761. [CrossRef] [PubMed]
22. Holm, A.; Mayr, S. Glassy and ballistic dynamics in collision cascades in amorphous TiO_2: Combined molecular dynamics and Monte Carlo based studies across energy scales. *Phys. Rev. B* **2021**, *103*, 174201. [CrossRef]
23. Chaikin, P.M.; Lubensky, T.C. *Principles of Condensed Matter Physics*; Cambridge University Press: Cambridge, UK, 1995.
24. Kaneko, K. Overview of coupled map lattices. *Chaos* **1992**, *2*, 279. [CrossRef] [PubMed]
25. Abramson, G.; Zanette, D.H. Globally coupled maps with asynchronous updating. *Phys. Rev. E* **1998**, *58*, 4454. [CrossRef]
26. Wolchover, N. Ideal Glass Would Explain Why Glass Exists at All. *Quanta Magazine*, 11 March 2020; pp. 1–6. Available online: https://www.quantamagazine.org/ideal-glass-would-explain-why-glass-exists-at-all-20200311/ (accessed on 2 August 2026).

Disclaimer/Publisher's Note: The statements, opinions and data contained in all publications are solely those of the individual author(s) and contributor(s) and not of MDPI and/or the editor(s). MDPI and/or the editor(s) disclaim responsibility for any injury to people or property resulting from any ideas, methods, instructions or products referred to in the content.